Editors' Suggestion

# Initial regime of drop coalescence

Christopher R. Anthony,* Michael T. Harris, and Osman A. Basaran†
*Davidson School of Chemical Engineering, Purdue University, 480 Stadium Mall Drive, West Lafayette, Indiana 47907, USA*

(Received 15 September 2019; accepted 20 February 2020; published 13 March 2020)

When two drops are slowly brought together and first touch, a microscopic liquid neck or a bridge forms between them. The expansion of the neck is controlled by the capillary (Laplace) pressure which diverges when the curvature of the interface is infinite at the point where the drops first touch. The change in topology and the flows that ensue as time advances and the bridge grows from microscopic to macroscopic scales, and the two drops merge into one, are intimately coupled to this singularity in the dynamics. Despite the large volume of work dedicated to this problem, currently experiment, theory, and computation are not in complete agreement with respect to the earliest times following the initial contact of the two drops. Experiments, supported by simulations, report an initial regime where the radius of the connecting bridge grows linearly in time before a transition to either a Stokes regime or an inertial regime where either viscous or inertial force balances capillary (surface tension) force. In the initial linear regime, referred to as the inertially limited viscous (ILV) regime, all three forces are thought to be important. This is in contrast to theory which predicts that all coalescence events begin in the Stokes regime where inertia is negligible. Here we use high-accuracy numerical simulations to show that the ILV regime is only realized when the two coalescing drops are initially separated by a finite distance. Moreover, for two drops that initially just touch at a point, coalescence always begins in the Stokes regime. It is demonstrated that the linear ILV regime is more akin to a Taylor-Culick-type regime whose existence and duration are purely consequences of the use of an initial bridge of finite size that poorly approximates the point contact condition that is a cardinal feature of the coalescence singularity.

DOI: 10.1103/PhysRevFluids.5.033608

## I. INTRODUCTION

Drop coalescence plays a central role in a variety of industrial and natural processes involving emulsions or dispersions of small drops of one fluid in a second, immiscible fluid [1,2]. In many processes encountered in the petroleum and the chemical industries, it is necessary to remove a dispersed water phase from a continuous oil phase. In the petroleum industry, water-in-oil emulsions are formed during the production of crude oil. If the oil is not dehydrated or demulsified, the presence of water in the oil can result in corrosion of pipes and other equipment, deactivation of catalysts, and increased costs in transporting the unwanted water by pipeline or tanker among other things [3]. In the petroleum industry, the application of electric fields to cause flocculation and coalescence of dispersed water drops has been widely adopted [4,5]. Also in both oilfield and refinery operations, electric fields are used first to atomize and then to coalesce water drops in

*anthonc@purdue.edu
†obasaran@purdue.edu

 

the desalting of oil [3]. While both electrically driven dehydration and desalting have been known for a century and are widely practiced but incompletely understood operations, electric fields have more recently been proposed for use in solvent extraction where the process of drop formation for generating increased surface area for mass transfer is followed by the operation of drop coalescence for affecting phase separation [6,7]. Similarly, the process in which electric fields are used to induce breakup followed by coalescence albeit while chemical reactions are occurring within microreactors composed of liquid drops has also been receiving increasing attention in diverse applications including the production of fine particles and powders [8].

Coalescence is also important in numerous other applications ranging from the food, agriculture, and consumer products industries to the manufacturing of advanced materials. For example, coalescence is a dominant process in determining the appearance as well as the shelf life of emulsion-based products including salad dressing and mayonnaise [9]. Drop collision and coalescence occur in dense spray systems and in particular in applications involving combustion [10]. In fuel injector systems, the competition between drop breakup and drop coalescence can have an impact on engine performance [11]. In the production of many solid-state materials including ceramics and metals, loose powders are fused together or sintered to form an interconnected solid [12]. At the particle scale, sintering of initially two spherical particles closely resembles the coalescence of two dispersion drops in an emulsion [13]. In polymer dispersions, the tendency of polymers to agglomerate is controlled by the introduction of stabilizer which seeks to limit droplet coalescence [14]. More recently, the controlled coalescence of drops in microfluidic devices has started to attract attention due to a host of potential applications in chemistry, biochemistry, and materials science [15].

In nature, the collision, bouncing, and coalescence of drops are central to raindrop growth and the development of thunderstorms and have captivated the attention of the atmospheric science community since the early studies of Benjamin Franklin and Lord Rayleigh [16,17]. Recently, Stone and coworkers [18] have reported that oppositely charged drops may not coalesce in strong electric fields. Also quite recently, researchers in the life sciences arena have studied and demonstrated the remarkable parallels between the coalescence of liquid drops and the fusion of membranes, vesicles, and nucleoli [19,20].

Consequently, due to its widespread prevalence in nature and use in industrial processes, there has been considerable amount of work done to understand the fundamentals of the coalescence of two drops (see below). The major goal of this paper is to advance the understanding of the dynamics of the coalescence of two drops in a dynamically passive exterior fluid during the earliest times following the instant when two drops have just touched and began to merge into one.

When two drops are slowly brought together and first touch, a microscopic liquid neck or a bridge forms between them. The expansion of the neck is controlled by the capillary (Laplace) pressure which diverges when the curvature of the interface is infinite at the point where the drops first touch. The change in topology and the flows that ensue as time advances and the bridge grows from microscopic to macroscopic scales, and the two drops merge into one, are intimately coupled to this singularity in the dynamics.

One of the earliest significant studies into how such a connecting bridge would grow and evolve in time was performed by Hopper [21,22] who obtained an exact analytical solution in the closely related problem of the coalescence of two infinitely long cylinders, i.e., two circles, in the creeping flow or Stokes limit. This two-dimensional (2D) analysis was extended to fully three-dimensional (3D) drops by Eggers *et al.* [23] who showed that the initial dynamics or the asymptotic behavior of two coalescing spheres (3D drops) is identical to that of two coalescing circles (its 2D counterpart). This regime of coalescence has come to be known as the Stokes regime where the growth of the connecting bridge follows a scaling law where the minimum radius of the neck $\tilde{R}_{\min}$ grows linearly in time $\tilde{t}$ albeit with a logarithmic correction, *viz.* $\tilde{R}_{\min} \sim -\tilde{t} \ln \tilde{t}$. The landmark paper by Eggers and coworkers has led to a flurry of numerical and experimental studies in the field [24–36].

However, some recent studies have called into question whether the Stokes or the viscous regime, where viscous and capillary (surface tension) forces alone are in balance while inertia is negligible,

is the initial regime of coalescence. Indeed, recent studies [29,31] suggest that an alternative regime wherein both viscous and inertial forces balance capillary force must be the initial regime of drop coalescence. This regime is referred to as the inertially limited viscous (ILV) regime in which the minimum bridge radius grows linearly with time without any logarithmic correction, *viz.* $\tilde{R}_{\min} \sim \tilde{t}$. That the ILV regime is the initial or asymptotic regime of coalescence has been demonstrated in both experiments [29,31] and simulations [29]. The lack of agreement between theory, which attests that the Stokes regime is the initial regime of coalescence, and experiment (supported by simulation) which instead purports that the ILV regime is the initial regime of coalescence, makes plain that a careful investigation of the possible reasons for this discrepancy and its resolution are worthy goals of research in drop coalescence and are the subjects of this paper.

The situation in which two drops of an inviscid fluid coalesce in a dynamically passive outer fluid has also received much attention. Scaling arguments in this limit predict a power law scaling in which the minimum radius of the connecting bridge depends on time to the one-half power [23,37], *viz.* $\tilde{R}_{\min} \sim \tilde{t}^{1/2}$. This behavior was shown to hold even with the occurrence of the creation of successive entrapped toroidal bubbles which had already been observed in previous numerical simulations [38] albeit with a modification to the prefactor in the scaling law. The existence of this inertial $\tilde{t}^{1/2}$ regime has been extensively validated through both experiments and simulations [24,26–29,31,34,35,37,39–41]. It is also noteworthy that during the coalescence of drops of liquids of small but finite viscosity, the dynamics will transition or crossover into this inviscid regime when the gap between the two drops, i.e., the axial separation between them, has grown sufficiently large so that it is comparable to the viscous length scale [28].

The paper is organized as follows. Section II describes the mathematical formulation of the problem along with the numerical method used in its solution. Section III uses simulations to analyze the initial regime of drop coalescence and determines whether the ILV or the Stokes regime is the true initial regime of coalescence. Section IV studies the dynamical transitions and/or regime changes that arise from the initial, or asymptotic, regime of coalescence to the inviscid regime. The paper ends in Sec. V with concluding remarks and a summary of possible areas in the field that can benefit from further study.

## II. MATHEMATICAL FORMULATION AND NUMERICAL METHOD

### A. Problem statement and mathematical formulation

The system consists of two identical liquid drops each of radius $\tilde{R}$ of an incompressible Newtonian fluid of constant density $\rho$ and constant viscosity $\mu$. Initially, the drops just touch at a point which, in the continuum mechanical analysis to be carried out in this paper, is replaced by that where the drops are connected by a microscopic bridge that is a cylinder of vanishingly small radius $\tilde{R}_0$ and vanishingly small height $2\tilde{Z}_0$ (see Fig. 1 and below). The drops are surrounded by a dynamically passive or inert exterior fluid, here taken to be a gas, e.g., air, that exerts a constant pressure on the drops. The surface tension $\gamma$ of the liquid-air interface separating the drop and the exterior fluid $S(\tilde{t})$ is spatially uniform and constant in time $\tilde{t}$. Initially, the fluid within the drops is quiescent so that the fluid velocity $\tilde{\mathbf{v}} = \mathbf{0}$ at time $\tilde{t} = 0$. In what follows, it proves convenient to adopt a cylindrical coordinate system $(\tilde{r}, \theta, \tilde{z})$ whose origin is located at the point where the drops initially just touch. Here $\tilde{r}$ and $\tilde{z}$ stand for the radial and axial coordinates and $\theta$ is the angle measured around the $\tilde{z}$ axis, with the $\tilde{z}$ axis running along the line connecting the centers of the two drops. Owing to the nature of the physical system that has just been described, the dynamics is taken to be axisymmetric about the $\tilde{z}$ axis or $\tilde{r} = 0$ and to be symmetric about the plane $\tilde{z} = 0$. Therefore, the problem domain, which is hereafter referred to as $\Omega(\tilde{t})$, is reduced to the single quadrant of the cross section of the interior of one drop or the 2D region that is bounded by the axis of symmetry $\tilde{r} = 0$, the plane of symmetry $\tilde{z} = 0$, and the liquid-air interface $S(\tilde{t})$.

Following earlier studies [29,42], the problem is nondimensionalized by taking the radius of the undisturbed drops as the characteristic length, $l_c \equiv \tilde{R}$, and the inertial-capillary time $t_{IC} \equiv \sqrt{\rho \tilde{R}^3/\gamma}$

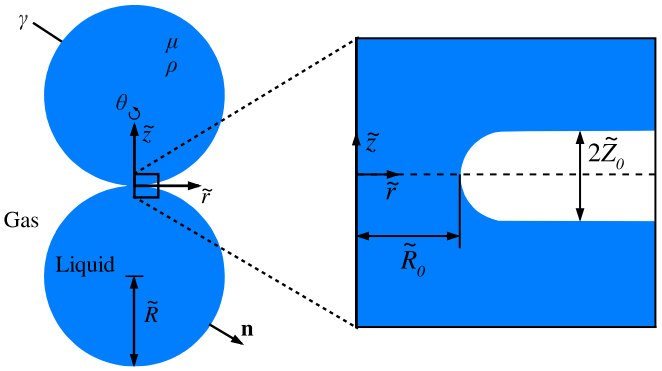


FIG. 1. The onset of the coalescence of two equal-sized drops in a dynamically passive exterior fluid, e.g., a gas such as air: definition sketch and initial conditions. At the initial instant $\tilde{t} = 0$, two spherical drops, each of radius $\tilde{R}$, are connected by a microscopic neck or bridge of radius $\tilde{R}_0$ and half height $\tilde{Z}_0$, a zoomed-in view of which is also shown (zoomed-in view not to scale). The fluid within the drops is quiescent at $\tilde{t} = 0$.

as the characteristic timescale, $t_c \equiv t_{IC}$. The ratio of these two scales is then used as the characteristic velocity, $v_c \equiv l_c/t_c$, and a scale based on the capillary pressure is taken to be the characteristic pressure/stress scale, $p_c \equiv \gamma/\tilde{R}$. Introduction of these scales into the problem reduces the number of governing parameters to just three dimensionless groups. The first is the Ohnesorge number, $\mathrm{Oh} \equiv \mu/\sqrt{\rho\tilde{R}\gamma}$, which is the ratio of the viscous force to the square root of the product of inertial and surface tension forces and is solely based on the physical properties and the radii of the drops. The other two dimensionless parameters arise because of the existence of a microscopic but finite-sized bridge that initially connects the two drops. These are the dimensionless bridge radius and height which are given by $R_0 \equiv \tilde{R}_0/\tilde{R}$ and $2Z_0 \equiv 2\tilde{Z}_0/\tilde{R}$. Henceforward, all variables without tildes over them are taken as the dimensionless counterparts of those with tildes, e.g., $r \equiv \tilde{r}/\tilde{R}$ is the dimensionless counterpart of $\tilde{r}$.

When two spheres just touch at a point, the equation locally describing the profiles of the two spheres is given by

$$z \approx \pm\tfrac{1}{2}r^2 + \cdots . \tag{1}$$

Therefore, locally, the surfaces of the two spheres resemble two kissing parabolas [35] and the distance between their surfaces varies as $r^2$. [Equation (1) is not used in the simulations carried out in this paper.] The point contact condition is replaced in the simulations by using an initial bridge of radius $R_0$ and height $2Z_0$ such that the equation of the surface of the bridge is given by

$$[r - (R_0 + Z_0)]^2 + z^2 = Z_0^2. \tag{2}$$

The point contact condition is well approximated by setting $2Z_0 = R_0^2$ and letting $R_0 \to 0$, which is hereafter referred to as the approximate point contact condition. In the following section, the effect of the size and aspect ratio of this finite connecting bridge, that is the value of $R_0$ and values of $2Z_0$ that do not necessarily equal $R_0^2$, on the coalescence dynamics is investigated.

The dynamics of drop coalescence, and the flow within the region $\Omega(t)$, is governed by the Navier-Stokes and continuity equations which in dimensionless form are

$$\frac{\partial \mathbf{v}}{\partial t} + \mathbf{v}\cdot\nabla\mathbf{v} = \nabla\cdot\mathbf{T}, \tag{3a}$$

$$\nabla\cdot\mathbf{v} = 0, \tag{3b}$$

where $\mathbf{T} \equiv \tilde{\mathbf{T}}/p_c = -p\mathbf{I} + \mathrm{Oh}[\nabla\mathbf{v} + (\nabla\mathbf{v})^T]$ is the dimensionless stress tensor, with $\mathbf{v} \equiv \tilde{\mathbf{v}}/v_c$ denoting the dimensionless fluid velocity, $p \equiv \tilde{p}/p_c$ is the dimensionless pressure, $t \equiv \tilde{t}/t_c$ is

dimensionless time, and $\nabla \equiv \tilde{R}\tilde{\nabla}$ is the dimensionless gradient operator. The pressure exterior to the drops is taken to be uniform in space and constant in time, and set to be the pressure datum.

The domain $\Omega(t)$ over which Eqs. (3a) and (3b) are solved consists of the region enclosed by the free surface $S(t)$, the shape and location of which are unknown *a priori*, the axis of symmetry $r = 0$, and the plane of symmetry $z = 0$. Symmetry boundary conditions are imposed along the latter two boundaries. Along the free surface $S(t)$, the kinematic and traction boundary conditions are applied to determine the unknown shape of the interface and to account for the discontinuity in stress due to surface tension:

$$\mathbf{n} \cdot (\mathbf{v} - \mathbf{v}_s) = 0, \tag{4}$$

$$\mathbf{n} \cdot \mathbf{T} = -2\mathcal{H}\mathbf{n}. \tag{5}$$

Here $2\mathcal{H} = 2\tilde{\mathcal{H}}\tilde{R}$ is twice the dimensionless local mean curvature of $S(t)$, $\mathbf{n}$ is the outward pointing unit normal to the free surface, and $\mathbf{v}_s = \tilde{\mathbf{v}}_s/v_c$ is the dimensionless velocity of points along the free surface $S(t)$.

### B. Numerical method

#### *1. ALE algorithm, spatial discretization, and time integration*

The aforementioned transient system of governing equations and boundary and initial conditions are solved numerically using a fully implicit, arbitrary Lagrangian-Eulerian (ALE) method of lines algorithm in which the Galerkin/finite element method (G/FEM) [43] is employed for spatial discretization [44] and an adaptive, implicit finite difference method is deployed for time integration [45]. In order to capture the large deformations that the surface of the coalescing drops or the free surface $S(t)$, and the domain $\Omega(t)$ enclosed by $S(t)$, undergo, the elliptic mesh generation method developed by Christoloudou and Scriven [46] for studying thin-film coating flows and which was later extended to simulate free surface flows of Newtonian and complex fluids with breakup and coalescence [29,45,47], is used to discretize the spatial domain $\Omega(t)$. With elliptic mesh generation, the radial and axial coordinates of each grid point in the moving, adaptive mesh are determined simultaneously with the velocity and pressure unknowns. The velocity and pressure unknowns are solved for in the mixed interpolation sense using biquadratic basis functions to represent the velocity unknowns and bilinear basis functions to represent the pressure unknowns [48]. The locations of the mesh coordinates are also represented using biquadratic basis functions. The numerical scheme reduces the problem to a system of nonlinear algebraic equations that can be solved iteratively via a multidimensional Newton's method. The resulting system of linear equations is then solved with a multifrontal algorithm which takes advantage of the sparsity of the Jacobian matrix that arises in Newton's method. This multifrontal algorithm is inspired by the frontal method introduced by Hood [49]. For a more complete description of the numerical method that has been employed, the reader is referred to Notz and Basaran [45] and Anthony *et al.* [50].

#### *2. Mesh construction and remeshing*

Simulating the coalescence of two drops entails solving a challenging multiscale free surface flow because of the occurrence of several disparate length scales. Indeed, the simulations require that the domain $\Omega(t)$ be discretized or subdivided into elements so that phenomena occurring over the following highly disparate length scales be accurately captured. First, there is the $O(1)$ length scale which is the radius of the undeformed drops. Next are two much smaller length scales: one is the $O(R_0)$ length scale which is the initial radius of the bridge or neck connecting the drops and another is yet even a smaller length scale, the $O(R_0^2)$ length scale which is the initial height of that bridge. Moreover, it will be seen below that another length scale arises that is of $O(R_0^3)$, making the range of length scales in the problem even more disparate. Indeed, if the initial bridge radius is

$O(10^{-4})$, phenomena that occur over length scales that differ by 12 orders of magnitude or a factor of $O(10^{12})$ must be dealt with in a given simulation.

To accomplish the goals stated in the previous paragraph, it is necessary to concentrate the elements of the mesh in the neighborhood of the connecting bridge. Although the elliptic mesh equations developed by Christodoulou and Scriven [46] use functions to concentrate the mesh where desired, it has been found necessary to incorporate additional, more strict methods of mesh concentration. Fortunately, since the overall dynamics of coalescence is rather predictable in that the connecting bridge will simply grow until the drops have merged, this fact can be exploited by incorporating into the mesh design an artificial algebraic surface that surrounds the neighborhood of the bridge and which grows with it in time. This has the effect of subdividing the domain and hence the mesh into two distinct parts such that elements from one side of the boundary are not permitted to cross into the other side. Given the physics of coalescence, it has been found convenient to construct this boundary as an ellipse that is specified solely by the minimum radius of the bridge, $R_{\min}(t)$, and whose shape is given by an equation that is determined by using Newton's method to force the ellipse to satisfy the conditions given by Eq. (6):

$$r_1 = 0, \tag{6a}$$

$$z_1 = \begin{cases} R_{\min}(t) & \text{if } R_{\min}(t) < 1/2 \\ 1/2 & \text{if } R_{\min}(t) \geqslant 1/2 \end{cases}, \tag{6b}$$

$$\left.\frac{\partial r}{\partial z}\right|_{(r_1,z_1)} = \tan(\pi/3), \tag{6c}$$

$$r_2 = 2R_{\min}(t), \tag{6d}$$

$$z_2 = 0, \tag{6e}$$

$$\left.\frac{\partial r}{\partial z}\right|_{(r_2,z_2)} = 0. \tag{6f}$$

An example mesh is shown in Fig. 2 at a relatively late stage of a simulation and depicts the division of $\Omega(t)$ into two domains by the algebraic surface that is marked in red. Elements in each subdomain are then concentrated where they are needed, e.g., near the neck, using the built in functionality present in the elliptic mesh equations. For computational efficiency, the movement of the algebraic surface is delayed by one time step relative to the current solution. This is done to avoid any dependency of the locations of the nodes along the algebraic surface on the node located at $r = R_{\min}$. Theoretically, this approach could be problematic if the algorithm were to take too large of a time step in situations in which $R_{\min}(t)$ is changing rapidly. However, the time step size determined by the adaptive time stepping algorithm used in the code, which is set by the instantaneous dynamics of the flow [45,48], is in practice always sufficiently small that this issue never arises.

While the strategy described in the previous paragraph has proven to be successful as $R_{\min}$ varies over a wide range, it does not perfectly control the mesh. When attempting to span many orders of magnitude in $R_{\min}$, typically three or more, the elements remain too concentrated in the bridge as the height of the bridge scales as $R_{\min}^2$ whereas the ellipse grows in proportion to $R_{\min}$. In order to accommodate large changes in the bridge size, periodic remeshing, typically whenever $R_{\min}$ increases by a factor of four, has been found convenient. In this remeshing step, the concentration imposed by the control functions in the elliptic mesh is relaxed to avoid having elements that are needlessly too small in the bridge. The accuracy of the remeshing process has been ensured by comparing and demonstrating excellent agreement between results obtained from simulations with remeshing and ones without remeshing. The remeshing coupled with the incorporation of an algebraic dividing surface in the domain has made it possible to carry out simulations over larger ranges of $R_{\min}$ than those reported in earlier works on drop and bubble coalescence [29,51]. A more detailed description of the aforementioned meshing techniques can be found in Ref. [52].

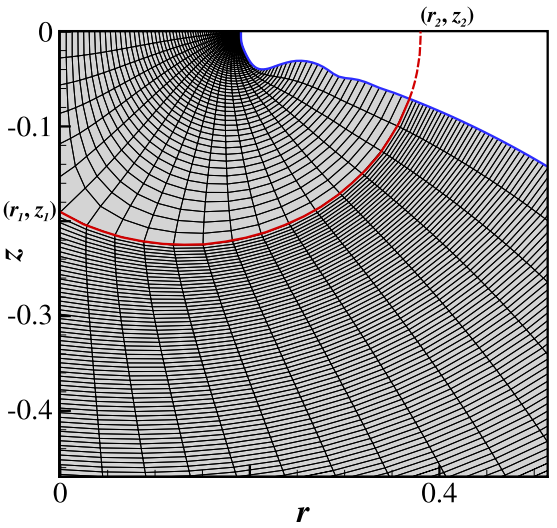


FIG. 2. Portion of an example mesh during the coalescence of two drops of Oh = 0.001 at the instant in time when $R_{\min} \approx 0.18$. The mesh is heavily concentrated both radially and axially near the neck compared to the bulk of the drop(s). The dividing surface or boundary, marked in red, moves according to an algebraic condition so that its position changes dynamically in time in response to the evolution of the bridge radius $R_{\min}(t)$, as discussed in the text. Actual simulations typically use a mesh that is two to four times more dense than the example shown here.

## III. INITIAL REGIME OF DROP COALESCENCE

As per the discussion in the introduction, it has come to be accepted based on some of the most recent experimental work in the field that coalescence always begins in the ILV regime and that the dynamics eventually transitions to either the Stokes regime if $\mathrm{Oh} \gtrsim 1$ or the inertial regime if $\mathrm{Oh} \lesssim 1$ [29] where the scaling law governing the variation of the minimum bridge radius $R_{\min}$ with time $\tau$ (see below) from the coalescence singularity is given in each of these regimes by

$$R_{\min} = -C_V \tau \ln\left(\frac{\tau}{\mathrm{Oh}}\right) \quad \text{(Stokes regime)}, \tag{7a}$$

$$R_{\min} = C_{ILV} \tau \quad \text{(ILV regime)}, \tag{7b}$$

$$R_{\min} = C_I \tau^{1/2} \quad \text{(Inviscid regime)}. \tag{7c}$$

$C_V$, $C_{ILV}$, and $C_I$ in Eqs. (7) are the prefactors in each of these three regimes. Moreover, the transition from the ILV to the Stokes regime is believed to occur when $\mathrm{Oh} \approx (R_{\min})^{-1/2} |\ln(\frac{R_{\min}}{8})|$ and the transition from the ILV to the inertial regime is believed to occur when $R_{\min} \approx \mathrm{Oh}$ [29]. Here, as we are particularly interested in demonstrating the existence or nonexistence of the ILV regime, the most instructive case to study is one that should not only begin in the ILV regime but also remain in the ILV regime during the entirety of the coalescence event. Thus, we consider the situation in which Oh = 0.6, which is also the primary case that was used to establish the existence of the ILV regime by Paulsen *et al.* [29]. While the dynamics in this case should theoretically transition from the ILV to the inertial regime when $R_{\min} \approx 0.6$, this value of $R_{\min}$ is large enough that finite-size effects would come into play when $R_{\min}$ has become so large and hence a transition between two scaling regimes would be difficult to observe in actuality. Moreover, because $\mathrm{Oh} < 1$ in this case, a transition to the Stokes regime would not be expected to occur.

Therefore, we now report results of simulations of drop coalescence when Oh = 0.6 and the point contact condition is approximated using Eq. (2) with $R_0 = 10^{-6}$ and $Z_0 = \frac{1}{2}R_0^2 = 5 \times 10^{-13}$.

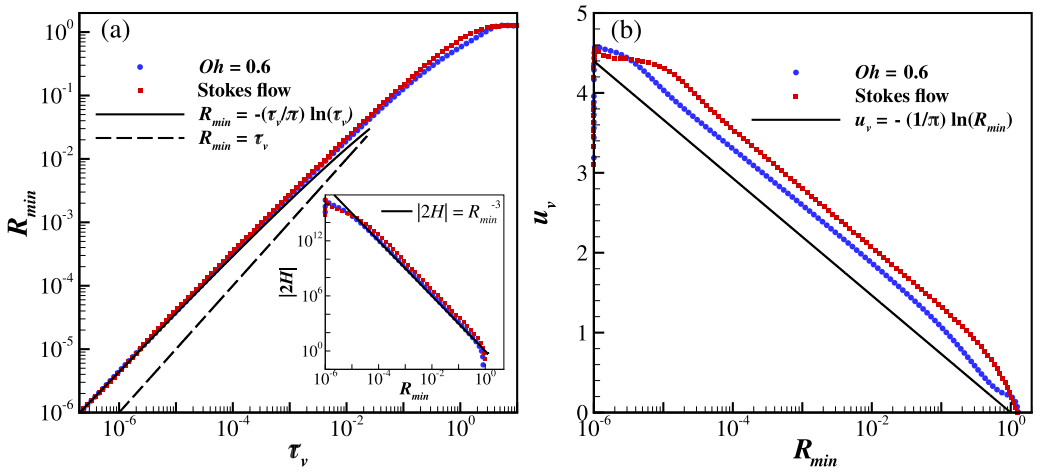


FIG. 3. Scaling behavior of three quantities obtained from simulations. (a) The variation of the minimum neck radius $R_{\min}$ with the viscous coalescence time $\tau_v$ (main figure) and the variation of the magnitude of twice the mean curvature $2\mathcal{H}$ with $R_{\min}$ (inset), both of which are shown as log-log plots. (b) The variation of the velocity of the growing neck or the bridge, which has been rescaled by the visco-capillary velocity, with $R_{\min}$ and which is shown as a semilog plot. In (a)–(b), it is demonstrated that the scaling laws inferred from the simulations closely follow the predictions obtained from Stokes theory for $R_{\min}$, $2\mathcal{H}$, and $u_v$ rather than those that would be expected in a linear ILV regime. Here Oh $= 0.6$, $R_0 = 10^{-6}$, and $Z_0 = (1/2)R_0^2 = 5 \times 10^{-13}$.

The use of such a small value for $R_0$, which is only made possible by the improved meshing scheme employed here, is to ensure that the simulations yield a sufficient amount of scaling data that can be fit by an equation such as those given in Eq. (7) before finite-size effects become important. Figure 3 shows the results of simulations in which the time evolution of the minimum bridge radius is depicted for two drops of Oh $= 0.6$ undergoing coalescence and also two purely viscous drops that are coalescing under Stokes flow conditions, i.e., simulations that have been carried out in the limit of $1/\text{Oh} = 0$.

Since simulations must begin when the bridge is already of finite size, in Fig. 3 the time coordinate has been redefined such that $\tau = t + t_{\text{con}}$. Here $t_{\text{con}}$ is the estimated time that has elapsed between the instant when the two drops just made contact and the time when the simulation began, $t$ is the time from the start of the simulation or the so-called simulation time, and the new time variable $\tau$ is the coalescence time which describes the total time since the occurrence of the space-time coalescence singularity. In order to determine the time since contact, simulation data are fit to a power law once $R_{\min}$ has increased by one order of magnitude and the contact time is determined by extrapolation of the data to zero bridge radius. This procedure is expected to work well for coalescence events that begin in a power law regime such as the ILV or the inertial regime. However, one would expect this procedure to give an inaccurate estimation of the time since contact in the Stokes regime. However, even with a poor determination of contact time or, worse yet, even if $t_{\text{con}} = 0$, only scaling results in the first decade of variation of $R_{\min}$ are affected until the true scaling regime takes hold. This initial transient or noise can be made smaller and smaller by starting the simulations at ever smaller values of $R_0$. Incidentally, this procedure is similar to that which is used in calculating the breakup or pinch-off time in studies of jet breakup (see Ref. [53]). Furthermore, since the simulation(s) in the Stokes limit should be scaled using the visco-capillary time $t_{VC} = \mu\tilde{R}/\gamma$ as characteristic time because density does not enter the problem in that limit, the simulation data at finite Oh (note that $\text{Oh} = t_{VC}/t_{IC}$) have also been rescaled accordingly where $\tau_v = \tau/\text{Oh}$ to enable comparison between simulations in which inertia is accounted for (finite Oh) and ones in which there is no inertia ($1/\text{Oh} = 0$ or $\text{Oh} = \infty$).

Upon the aforementioned rescaling, we see in Fig. 3(a) that the simulation results at a finite value of Oh overlap with or collapse onto both the simulation results carried out assuming the fluid within the drops is undergoing Stokes flow and the theoretical prediction of Eggers *et al.* [23] where $R_{\min} = -(\tau_v/\pi)\ln(\tau_v)$ which is valid for $R_{\min} < 0.03$. By contrast, the linear scaling behavior expected from the ILV regime is a relatively poor fit to the simulation data for all times regardless of the value of the prefactor chosen. Although the distinction between the Stokes and the ILV regimes is quite clear here given the large range of $R_{\min}$ spanned by the simulations carried out in this paper, it is often more instructive and/or useful to derive the radial scaling behavior from the scaling of the radial velocity at the location of $R_{\min}$, *viz.* $u_{\min} = u(r = R_{\min})$. Figure 3(b) shows the variation of the rescaled velocity, which has once again been rescaled by using the visco-capillary timescale such that $u_v = u_{\min}\mathrm{Oh}$, with $R_{\min}$. This figure provides a definitive test as to which regime is the initial regime of coalescence and a clear delineation between them because on a log-log plot the inertial scaling regime would yield a straight line with a slope of $-1/2$, on a semilog plot the Stokes regime would yield a straight line with slope $1/\pi$, and the ILV regime would be represented by a horizontal line on either plot because the velocity is a constant in that regime. Figure 3(b) makes plain that on a semilog plot, both the simulation data for Stokes flow and the simulation data for $\mathrm{Oh} = 0.6$ yield straight lines as would be expected in a Stokes regime. Moreover, the slopes of the lines from the two simulations are identical with the predicted slope of $1/\pi$ from theory. Any small discrepancy at late times may be due to finite-size effects and/or the onset of the transition out of the Stokes regime into the inviscid regime.

The driving force for coalescence and hence the resulting flows in this problem is due to the large curvature of the meniscus in the vicinity of $r = R_{\min}$. In theoretical analyses of coalescence and in the derivation of the scaling law for coalescence in the Stokes regime, a scale that is smaller than the bridge height, $2Z_b \approx R_{\min}^2$, arises. This small length scale is given by $\delta \approx R_{\min}^3$ [23], and represents the scale of a radially directed ring force that drives the coalescence process. Therefore, we next test whether the simulations can accurately predict this small length scale by obtaining from simulation data how the magnitude of twice the mean curvature of the interface $|2\mathcal{H}|$ scales in this locale keeping in mind that the expectation from theory is that $|2\mathcal{H}| \approx \delta^{-1} \approx R_{\min}^{-3}$. The inset to Fig. 3(a) clearly shows that the numerically computed values of $|2\mathcal{H}|$ in both the finite and infinite Oh simulations do indeed scale with $R_{\min}^{-3}$ as expected from theory. That this scaling is observed in either case and that an ultrasmall length scale $\delta$ does indeed exist provides yet more credence that coalescence does indeed begin in the Stokes regime (also, see below). Moreover, because this length scale was predicted by Hopper to be of central importance in the similarity solution for the interface profile during coalescence of two infinite cylinders [22], we have constructed similarity profiles by suitably collapsing the transient profiles obtained from the solutions of the Navier-Stokes system. Here the collapse of the numerical solutions is accomplished by rescaling of the radial and the axial length scales by $R_{\min}$ and $R_{\min}^2$, respectively. This collapse is demonstrated in Fig. 4 where the rescaled shape profiles are plotted over five orders of magnitude of variation in $R_{\min}$.

Given that the new simulations when $\mathrm{Oh} = 0.6$ show that the initial dynamics clearly lies in the Stokes regime, it is natural to ask why a linear regime was observed in both the experiments and the simulations in Ref. [29]. It is worth noting that a key difference between their simulations and the ones being presented here pertains to the initial geometry of the bridge or, more precisely, how the value of half the bridge height $Z_0$ is assigned in this paper as opposed to that in Ref. [29]. The results presented in Fig. 3 have been obtained using an initial half bridge height of $Z_0 = (1/2)R_0^2$ whereas in the previous simulations in Ref. [29] a value of $Z_0 = 0.1R_0$ was used due to computational limitations. This limitation inherent to the computational results reported in Ref. [29] was necessitated because simulations become increasingly more difficult as $Z_0$ is decreased from a value that is comparable to or somewhat smaller than $R_0$ to a value that scales as $O(R_0^2)$ and hence is orders of magnitude smaller than the initial bridge radius when $R_0 \ll 1$. Therefore, if $R_0 = 10^{-3}$, while the value of $Z_0$ used here would be $5 \times 10^{-7}$, that used in Ref. [29] was $10^{-4}$. Given the large discrepancy of more than two orders of magnitude in the initial gap width between the two works, a study is undertaken into any possible effect that the gap width or bridge height can have on the

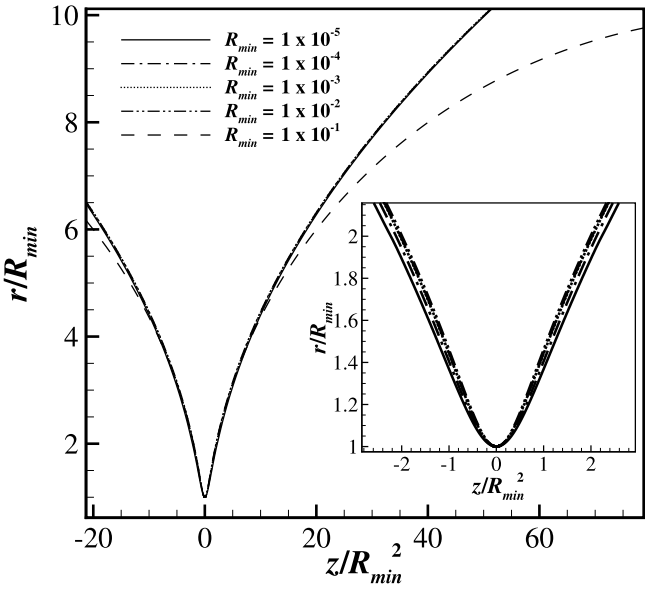


FIG. 4. Variation of the appropriately scaled profiles of the bridge or neck connecting two coalescing drops as a function of the minimum radius $R_{\min}$ and hence time. The profiles are seen to collapse nicely onto a single similarity profile as $R_{\min} \to 0$. The inset shows a blow-up of the interface profiles shown in the main figure by focusing in on the region in the vicinity of the location where the bridge radius is a minimum. Here Oh $= 0.6$, $R_0 = 10^{-6}$, and $Z_0 = (1/2)R_0^2 = 5 \times 10^{-13}$.

scaling dynamics by carrying out simulations over the range of values of $5 \times 10^{-7} \leqslant Z_0 \leqslant 10^{-4}$. (It should be noted that whereas values of $R_0$ as small as $10^{-6}$ and values of $Z_0$ as small as $5 \times 10^{-13}$ have been used in this paper, the smallest values of these length scales that could be achieved in Ref. [29] were $10^{-3}$ and $10^{-4}$, respectively.)

Figure 5 shows simulation results for the scaling of $R_{\min}$ with time $t_v$ where the latter has again been rescaled with the visco-capillary time, *viz.* $t_v \equiv \tilde{t}/t_{VC} = t/\mathrm{Oh}$. The results shown in this figure make clear that as the initial value of the half bridge height is increased from the ideal case of two drops starting to coalesce from an initial state of approximate point contact, *viz.* $Z_0 = 5 \times 10^{-7}$, the simulation results depart from what would be expected in the Stokes scaling regime and the early time dynamics begin to exhibit behavior that would be expected in an apparent initial linear regime. The duration of this linear regime is dependent on the value of $Z_0$ and once sufficient time has elapsed, this regime ends and thereafter the dynamical response exhibited by all simulations collapse onto that which would be expected in the Stokes regime. It is noteworthy that the case of $Z_0 = 10^{-4}$ reported in this figure is identical to the case that was used in Ref. [29] to demonstrate the existence of the ILV regime and that the results obtained in this work and those reported in Ref. [29] are in good agreement with each other when a consistent set of initial conditions, *viz.* $R_0 = 10^{-3}$ and $Z_0 = 0.1R_0 = 10^{-4}$, are used despite the improved meshing scheme and higher resolution simulations that are utilized in this work. The inset to Fig. 5 shows the computed scaling of the half bridge height $Z_b$, which is calculated from the simulations as $Z_b = z(r = 1.05R_{\min})$ and which is expected to scale as $R_{\min}^2$ given the geometry of the two drops. However, when the drops are connected by a bridge of finite height, *viz.* $Z_0 > (1/2)R_0^2$, the height of the bridge grows insignificantly in time compared to the initial separation between the drops. This delayed or arrested growth in the instantaneous height of the bridge lasts longer as the value of $Z_0$ is increased.

A similar situation arises and has already been reported in bubble coalescence when a finite bridge connects the two bubbles [42]. (We note that in the most recent and accurate simulations

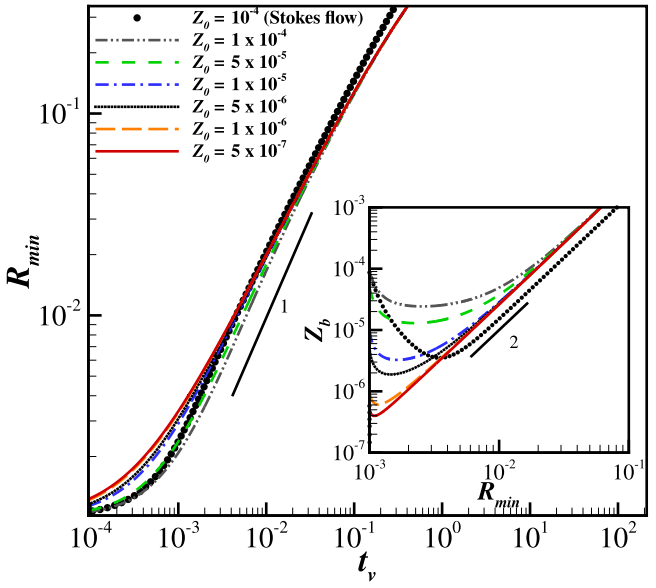


FIG. 5. The effect of the initial half bridge height $Z_0$ on the variation with time of the instantaneous value of the minimum radius $R_{\min}$ (main figure) and the variation of the instantaneous value of the half bridge height $Z_b$ with $R_{\min}$ (inset). Here all simulations begin with an initial bridge of radius $R_0 = 10^{-3}$ but the initial bridge height in the different simulations is systematically increased from the case where two drops virtually touch at a point, *viz.* $Z_0 = (1/2)R_0^2$, to values where $Z_0$ approaches $0.1R_0$. Lines/curves represent simulation results when Oh $= 0.6$, whereas symbols denote the results of a Stokes flow simulation in which $Z_0 = 0.1R_0 = 10^{-4}$. A line of slope one in the main plot shows that a linear regime in radial scaling is followed until the axial scale $Z_b$ begins to vary as $R_{\min}^2$ as shown in the inset.

of bubble coalescence [42], it has been demonstrated that simulations and theory are in excellent agreement when proper initial conditions on the bridge connecting the two bubbles are used in the computations.) As in the case of bubble coalescence, the dynamics in the present case can also be understood as a Taylor-Culick [54,55] regime that is analogous to the retraction of a gas film that has undergone point rupture. When this linear regime should give way to the Stokes regime can be predicted by equating the value of $Z_0$ to the value of the half bridge height in the ideal case as a function of $R_{\min}$, that is, $Z_b = (1/2)R_{\min}^2$. One can then solve for the value of $R_{\min}$ where the increase in bridge height due to the curvature of the drop surfaces has become equal in magnitude to the initial separation of the drops, giving a value of a crossover radius of $R_c = (2Z_0)^{1/2}$. Once this crossover radius has been reached, the dynamics forgets the finiteness of the initial bridge height and thereafter the scaling of $Z_b$ with time follows that in the ideal case. The results reported in Fig. 5 confirm that this is indeed what is observed and that the simple estimate for the duration of the linear regime is also consistent with the simulation results. Therefore, these findings suggest that the ILV regime is simply a consequence of the initial conditions that give rise to a Taylor-Culick regime where the axial scale is roughly constant, which is a point that is returned to below. Furthermore, Fig. 5 includes the results from one simulation, which are shown as symbols, that has been carried out under Stokes flow conditions with $Z_0 = 10^{-4}$ and which clearly shows that the dynamics in this case too follows the Taylor-Culick regime for some time as well. Since the inertial terms have been thrown out or set equal to zero in the Stokes flow simulation, the resulting scaling regime must truly be due to the finite size of the initial bridge connecting the drops and not the existence of the ILV regime where inertial and viscous forces would balance capillary force.

Armed with the realization that the ILV regime is akin to a Taylor-Culick-type regime, we show in Fig. 6 the variation of the absolute value of twice the mean curvature $|2H|$ in the vicinity of

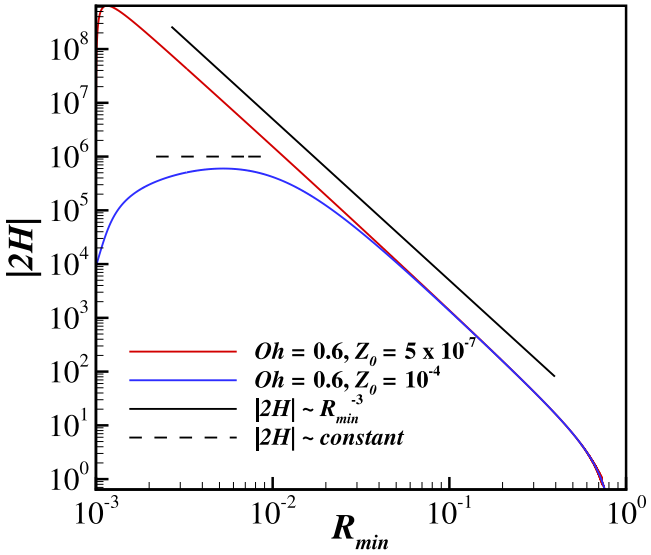


FIG. 6. Scaling of the curvature in the Stokes and the ILV regimes. The variation of the magnitude of twice the mean curvature $2\mathcal{H}$ with $R_{\min}$ determined from simulations. In both cases, Oh $= 0.6$ and $R_0 = 10^{-3}$. In one of the cases (red curve), the simulations have been carried out with an initial condition of an ideal bridge or a virtually point contact initial condition where $Z_0 = (1/2)R_0^2 = 5 \times 10^{-7}$. In the other case (blue curve), a finite-size bridge is used as an initial condition where $Z_0 = 0.1R_0 = 10^{-4}$. In the first case, the dynamics follows that which is expected in the Stokes regime (black line of slope of $-3$.) In the second case, the dynamics follows ILV scaling at early times where the curvature is nearly constant (dashed black line) for some time. In the latter case, the dynamics ultimately transitions to the Stokes regime at late times (and/or for large values of $R_{\min}$) where $|2H|$ once again scales as $R_{\min}^{-3}$.

the neck with the minimum neck radius $R_{\min}$ in two situations in which Oh $= 0.6$. One of the cases shown depicts the results of a simulation that has been carried out with an initial bridge corresponding to the situation where two drops virtually touch at a point (ideal condition where $Z_0 = (1/2)R_0^2 = 5 \times 10^{-7}$) whereas in the other case, the simulation has been performed with an initial bridge of finite size that poorly approximates the point contact condition ($Z_0 = 0.1R_0 = 10^{-4}$). In the former case, the dynamics lies in the Stokes regime and $|2H| \sim R_{\min}^{-3}$, in agreement with earlier results. However, in the latter case where the dynamics initially follows ILV scaling, after the decay of initial transients, the curvature becomes virtually constant for some time, in accordance with a Taylor-Culick-type behavior. Therefore, using the $1/R_{\min}^3$ scaling of curvature as a yardstick is indeed one of several reliable measures for ascertaining whether or not coalescence is occurring in the Stokes regime.

It is worth noting that the retracting neck and the air film may succumb to azimuthal or 3D instabilities, as in Ref. [56] where retraction of a fluid sheet in a viscous atmosphere is studied (see also Ref. [57]). However, as in other computational studies of drop coalescence to date (e.g., Refs. [23,29,32]), we leave the possibility of such azimuthal instabilities as an open problem for future research in fluid mechanics.

## IV. SCALING TRANSITIONS IN DROP COALESCENCE

While it has been established in the previous section that the initial regime of coalescence is indeed the Stokes regime, scaling regime transitions are expected to occur that depend on the value of the Ohnesorge number. To search for these transitions, a study is undertaken in this section on the effect of Oh on the scaling dynamics by varying the Ohnesorge number over the range

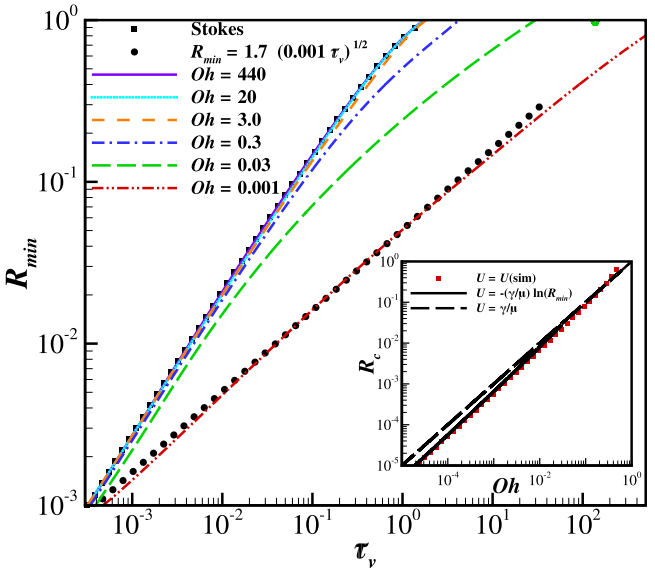


FIG. 7. Scaling behavior or the variation with the viscous coalescence time $\tau_v$ of the minimum neck radius $R_{\min}$ on a log-log plot for a range of values of Oh indicated by the various line types in the legend of the main figure. The simulation results show that that in all cases (except when Oh $= 10^{-3}$ where the dynamics is already in the inviscid regime), coalescence begins in the Stokes regime and the variation of $R_{\min}$ with $\tau_v$ closely follows that observed in the Stokes flow simulation (indicated by the square data points) until the crossover radius $R_c$ is reached. Thereafter, the dynamics transitions to the inviscid regime where $R_{\min}$ exhibits a power law scaling in $\tau_v$ with a slope of $1/2$. The data points that are circles correspond to a straight line of slope $1/2$ on the log-log plot as indicated in the legend. The results for Oh $= 440$, 20, and 3 are virtually indistinguishable from the results of the Stokes flow simulation, i.e., the curves representing these large but finite Oh cases lie on top of the data points corresponding to the Stokes flow case, over the entire time range shown. A relation for $R_c$ is shown in the inset with both the linear dependence of Ref. [28] ($U = \gamma/\mu$) and the logarithmic corrections suggested here that are derived from theory [$U = -(\gamma/\mu)\ln(R_{\min})$] and simulation data [$U = U(\text{sim})$]. Here all simulations start with an initial bridge of $R_0 = 10^{-3}$ and $Z_0 = (1/2)R_0^2 = 5 \times 10^{-7}$.

$10^{-3} \leqslant \text{Oh} \leqslant \infty$. All simulation results that are presented in the remainder of this paper have been carried out using the ideal case in which at the initial instant there is approximate point contact between the two drops, *viz.* $Z_0 = (1/2)R_0^2$. A crossover from the Stokes regime to the inviscid regime is expected to occur when the local Reynolds number in the neck, which is given by $\text{Re} = \rho U L/\mu$ where $L$ is the local length scale and $U$ is local velocity scale, becomes unity. Recent experimental studies [28,29] have shown the crossover radius $R_c$ for the transition from the Stokes regime to an inertial regime depends linearly on Oh. This result can be arrived at by taking the relevant length scale and the velocity scale to equal the instantaneous bridge height $R_{\min}^2$ and the instantaneous velocity of the growing bridge $u_{\min}$ [28] (but see the following paragraph). Figure 7 shows that when $R_{\min}$ is plotted against $\tau_v$, in all of the simulations, with the exception of the case when Oh $= 0.001$, the time evolution of the minimum bridge radius exhibits near perfect overlap with that obtained from the Stokes flow simulation. While all simulations for Oh $> 1$ remain in the Stokes regime for the entire period shown in the figure, the dynamics for both Oh of 0.03 and 0.3 can be seen to exhibit a departure towards the inviscid regime where $R_{\min} \approx \tau^{1/2}$ as time increases. Although both cases of Oh $= 0.03$ and 0.3 appear to transition to the inviscid regime in accordance with $R_c \approx \text{Oh}$, the transition is particularly evident for the case of Oh $= 0.03$. These results further affirm the linear relation between the crossover radius and Ohnesorge number found in recent studies [28,29] and is in contrast to earlier studies which had suggested a crossover radius that varied with Ohnesorge number as $R_c \approx \text{Oh}^2$ [23,26,27,37,41,58].

While the transitions shown in Fig. 7 do seem to follow the linear dependence of the crossover radius on Ohnesorge number, $R_c \approx \mathrm{Oh}$, this relation was obtained assuming that the local velocity is constant and equal to the visco-capillary velocity as in the ILV regime whereas it has been shown here that the bridge radius grows in time with a logarithmic correction. Therefore, if one instead takes $L = \tilde{R} \times R_{\mathrm{min}}^2$ (as earlier) and $U = -(\gamma/\mu)\ln(R_{\mathrm{min}})$ (rather than the constant velocity used earlier), a relation between the Ohnesorge number and the crossover radius can be derived as $\mathrm{Oh}^2 = (R_c^2)|\ln(R_c)|$. However, this relation should only be used for $\mathrm{Oh} < 0.03$ since the expression for the velocity is limited to this range. This limitation can be avoided and the estimation of the crossover radius can be extended to later times, and hence larger values of the crossover radius, by instead obtaining $U$ directly from a simulation of drop coalescence under Stokes flow conditions. The inset to Fig. 7 shows that when the crossover radius with the logarithmic correction is plotted against the previously discussed linear relation, the value of the predicted crossover radius is relatively unchanged over the range investigated in the main part of the figure. For example, the value of the crossover radius predicted with the improved method approximately equals 0.028 when $\mathrm{Oh} = 0.03$. Remarkably, even the improved value of the predicted crossover radius for $\mathrm{Oh} = 3.5 \times 10^{-6}$ differs from the original prediction by a factor of one-half. While it is desirable to attempt to verify the relation predicting the value of the crossover radius at lower values of Oh, the reconnection phenomenon described by Duchemin *et al.* [37] is more likely to occur at lower values of both $R_{\mathrm{min}}$ and Oh. The exploration of such cases proves prohibitive as it is not possible to continue the simulations after a reconnection occurs with the algorithm that is used in this work.

Although considerable effort has been expended up until this point to thoroughly examine the dynamics in the vicinity of the singularity and to identify the scaling behavior displayed by the growing bridge, it is also instructive to analyze the dynamics that are occurring on a larger scale within the coalescing drops. While it would be expected that the flow profiles would be qualitatively different in the inviscid and Stokes regimes, it was further shown in Ref. [29] that a different type of flow field arises for intermediate values of Oh where the ILV regime was believed to occur. Clearly, a question of central importance is whether the specific details, i.e., radius and height, of the initial finite-sized bridge connecting the two drops has any impact on the flow profiles on a large scale in addition to modifying the scaling behavior that is exhibited by the neck. In order to answer this question, the results of three simulations, two at finite Ohnesorge numbers of $\mathrm{Oh} = 10^{-3}$ and 0.6 and the third under Stokes flow conditions, are compared in Figs. 8(a)–8(c). These flow profiles do appear to indicate the occurrence of three distinct flow regimes and are for all practical purposes identical to those reported by Paulsen *et al.* [29] who used these distinct flow profiles as evidence for the existence of the third regime, the ILV regime. According to Paulsen *et al.*, the unique trademark of the ILV regime is the large recirculations seen in Fig. 8(b) for $\mathrm{Oh} = 0.6$ but which are absent in the Stokes flow simulation shown in Fig. 8(c). It is also noteworthy that the case of $\mathrm{Oh} = 0.001$ is indicative of the inviscid regime where capillary waves can be seen to be propagating along the interface from the bulge that is clearly visible in Fig. 8(a) in the vicinity of the bridge.

Since there still appears to be three distinct types of behavior when the dynamics is viewed on a larger scale than that of the growing bridge, it is helpful to categorize these coalescence events using an approach that was developed in Ref. [29]. In that work, the motion of the back of the drop that is farthest from the coalescence singularity was tracked by measuring both experimentally and computationally the axial velocity $V_{b.o.d.}$ at that point. In the inviscid regime, capillary waves that emanate from the growing bridge should propagate to the back ends of the drops and cause an oscillatory response in time. By contrast, in the Stokes regime, a force balance can be carried out to infer the center-of-mass motion of the drops and thereby used to show that $V_{b.o.d.} = \frac{\mathrm{Oh}}{2\pi} R_{\mathrm{min}} |\ln(R_{\mathrm{min}}/8)|$ [29]. Figure 8(d) shows the aforementioned oscillatory behavior when $\mathrm{Oh} = 0.03$ and where the drop has already entered the inviscid regime while the simulation results for Stokes flow follow closely the prediction obtained from the theoretical expression reported above [29]. What is perhaps more interesting is that for cases of intermediate Oh, there is a region of super linear growth that precedes the collapse of the data onto the Stokes flow simulation and the theoretical expression derived in Ref. [29]. However, when $\mathrm{Oh} = 0.6$, the flow field does

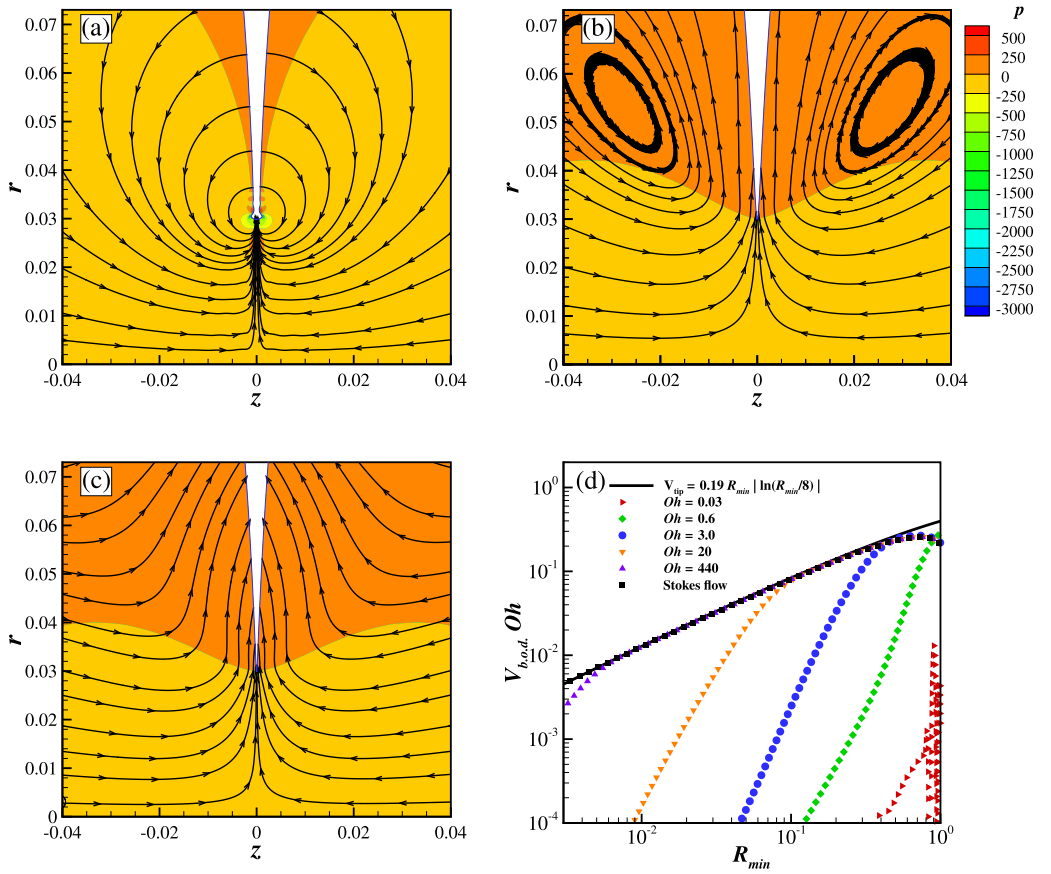


FIG. 8. Instantaneous flow fields and pressure contours within the drops at the instant in time when $R_{\min} = 0.03$ for the situations in which (a) $\mathrm{Oh} = 10^{-3}$, (b) $\mathrm{Oh} = 3 \times 10^{-2}$, and (c) $1/\mathrm{Oh} = 0$ or $\mathrm{Oh} = \infty$ (Stokes flow). Although there are only two distinct scaling regimes governing the time evolution of the neck in the vicinity of the space-time singularity, the global dynamics can exhibit three qualitatively different types of flows. (d) The existence of three different types of global flow fields is further demonstrated by monitoring the instantaneous value of the axial velocity of the back of the drop(s), $V_{b.o.d.}$. Here simulation results for a range of Oh (shown by different symbols) are compared to predictions from Stokes flow theory (shown by the black line). All simulations start with an initial bridge of $R_0 = 10^{-3}$ and $Z_0 = (1/2)R_0^2 = 5 \times 10^{-7}$.

not approach that which arises in the Stokes flow limit until the coalescence event is essentially completed despite the fact that Fig. 3 clearly shows that the local dynamics in this case lies in the Stokes regime during the entirety of the coalescence event. This transition from super linear growth onto the response that is exhibited by two drops undergoing Stokes flow has been used in the past as additional justification for the existence of the ILV regime and also as an indicator or a signal for the transition between the ILV and Stokes regimes. In summary, while it has been demonstrated in this paper that the dynamics that is local to the vicinity of the small region of the growing bridge may only fall into either the inviscid or the Stokes regime, flows that arise on the scale of the drop radii may in fact lie in one of three possible regimes, i.e., inertial, viscous (Stokes), or inertial-viscous.

Interface profiles obtained from transient simulations at any Ohnesorge number may be shown to collapse onto a similarity profile by suitably rescaling the radial coordinate by $R_{\min}(t)$ and the axial coordinate by $R_{\min}^2$, and plotting the rescaled profiles that have thereby been obtained at a number of instants in time as $R_{\min} \to 0$. This collapse was demonstrated earlier for the coalescence of two drops when $\mathrm{Oh} = 0.6$. It is also instructive to perform a similar exercise by rescaling

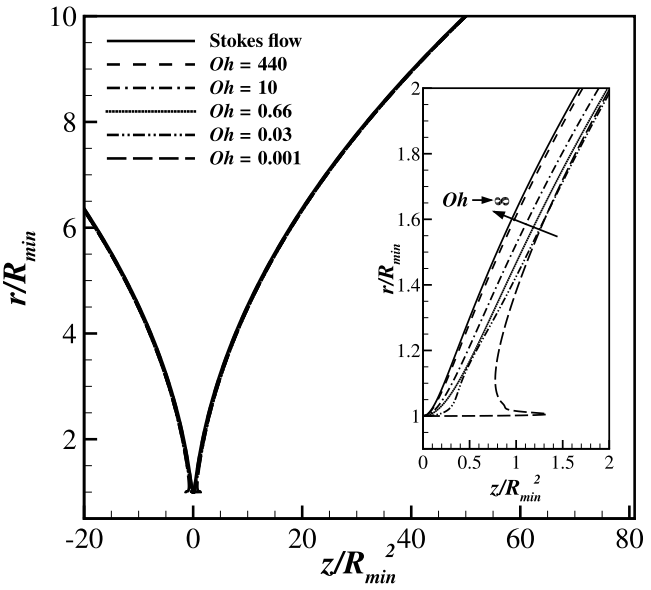


FIG. 9. Variation with Oh of the appropriately scaled profiles of a growing bridge connecting two coalescing drops as Oh $\to \infty$ at the instant in time when $R_{\min} = 8 \times 10^{-3}$. As Oh $\to \infty$, the profiles are seen to collapse or tend nicely onto a single similarity profile that results in the limit of Stokes flow. When Oh $\ll 1$, the scaled interface shape takes on a starkly different profile with a characteristic bulge indicative of the inviscid regime. The inset shows a zoomed-in view of the neck or the tip of the receding air film. Here $R_0 = 10^{-3}$ and $Z_0 = (1/2)R_0^2 = 5 \times 10^{-7}$ in all simulations.

interface shapes obtained from simulations at different values of Oh and examining the collapse of such profiles onto the limit as Oh $\to \infty$. While all such solutions would collapse onto the Stokes solution as $R_{\min} \to 0$, it is equally instructive to compare such rescaled profiles obtained at different values of Oh at the same value of $R_{\min}$. Therefore, rescaled profiles when $R_{\min} = 8 \times 10^{-3}$ obtained from simulations at different values of Oh are shown in Fig. 9 and demonstrate a clear collapse or approach of the profiles at different values of Oh to that of Oh $\to \infty$ (Stokes flow). When the inset to the figure is examined more closely, the rescaled profile for Oh $= 10^{-3}$ can be seen to deviate quite dramatically from all the others. This difference is expected since at this value of $R_{\min}$, the case of Oh $= 10^{-3}$ is the only one which lies in the inviscid regime as made evident by the large bulge in the interface profile that is characteristic of the inviscid regime (cf. Refs. [24,37]) in contrast to the other cases which all exhibit the slender profile that is characteristic of the Stokes regime. To further highlight the difference between the two regimes, Fig. 10 depicts interface profiles for the same cases as in Fig. 9 albeit where the two axes have been scaled in a different way than that in the previous figure. First, in Fig. 10(a) the radial coordinate has been shifted so that tip of the blob in the inviscid regime is located at (0,0) and both the radial and axial coordinates have been scaled by $R_{\min}^2$ to demonstrate that the extent of the bloblike tip of the retracting air film is roughly two in both directions. The latter point is reiterated in Fig. 10(b), which shows that the apparently sharp corner in the interface profile when Oh $= 0.001$ in Fig. 9 is indeed due to the rescaling of the axes and the actual interface profile near the tip is smooth when plotted with respect to physical coordinates (both of which, however, have been scaled by the minimum radius).

## V. CONCLUSIONS

Through a detailed exploration by means of high-accuracy simulation of the dynamics of two coalescing drops, the discrepancy that had existed between experiments [35] and theory [23] on

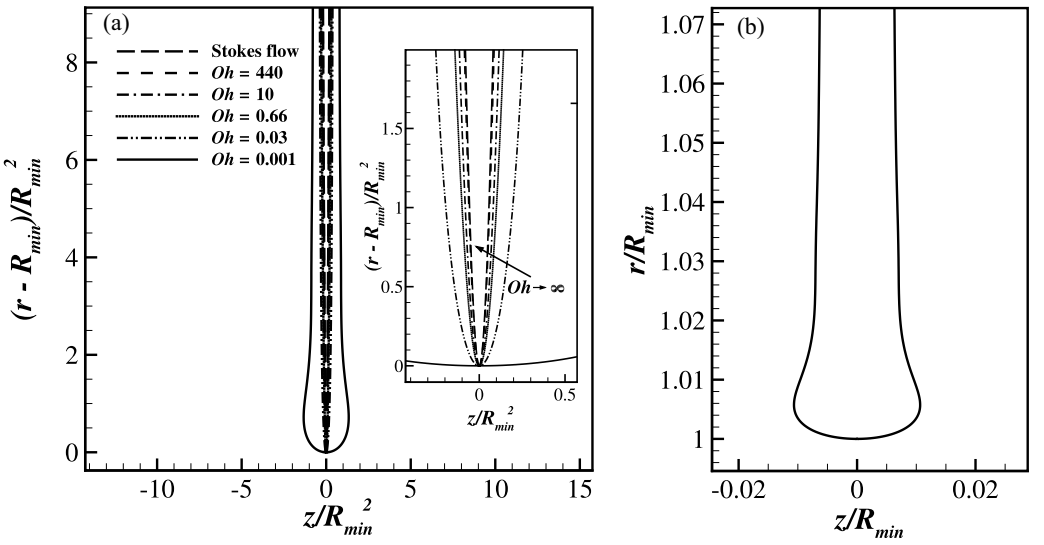


FIG. 10. Profiles of a growing bridge between two coalescing drops for the same set of Oh and at the same instant in time as in Fig. 9. (a) Interface profiles are shown after the radial coordinate has been shifted as explained in the text. Here both the shifted radial coordinate and the axial coordinate are then normalized by $R_{\min}^2$ to highlight the blob in the situation in which the Ohnesorge number is smallest (Oh = 0.001) and that the blob is of nearly equal $O(1)$ extent in both the radial and the axial directions. The inset shows a zoomed-in view of the neck or the tip of the receding air film. (b) The interface profile when Oh = 0.001 that further highlights the blob that forms in the inviscid limit.

the initial regime of coalescence has been resolved. Previously, experiments had indicated that all coalescence events should begin in the inertially limited viscous, or ILV, regime before transitioning to either the Stokes regime or the inviscid regime depending on the value of the Ohnesorge number, whereas theory had shown that coalescence should begin in the Stokes regime before transitioning to the inviscid regime. In simulations presented here, it has been shown that coalescence always begins in the Stokes regime, thereby demonstrating excellent agreement between theory and simulation for values of $R_{\min}$ as small as $10^{-6}$. Simulations have shown that the ILV regime does not arise regardless of the value of $R_{\min}$ or Oh. Moreover, with the simulation results presented in this paper, it has been further affirmed that the crossover radius between the initial Stokes regime and the inviscid regime should indeed have a linear dependence on Oh and is clearly more accurate than the previously held notion that it should vary as the square of Oh. Moreover, small logarithmic corrections to the linear crossover expression have been suggested here that improve the accuracy of the expression particularly for small values of Oh. Using all of this information, a phase diagram showing the regimes of coalescence of drops in air as well as transitions between them can be constructed that summarize succinctly the results obtained in this work as shown in Fig. 11. Here the transition between the Stokes and inviscid regimes is determined by using as the velocity of the growing bridge the value that is obtained directly from simulations and by taking as the appropriate length scale the bridge height or $R_{\min}^2$. The crossover radius at a given value of Oh is then calculated by determining the point at which the local Reynolds number of the flow becomes unity, as has already been done earlier in Fig. 7. It has further been shown that the crossover radius can also be estimated well by using the relation $\mathrm{Oh}^2 \approx (R_c^2)|\ln(R_c)|$, which is valid so long as $R_{\min} \leqslant 0.03$, and the estimate that is thereby obtained is found not to differ significantly from the previously established relation of $R_c \approx \mathrm{Oh}$ that had been deduced in earlier studies [28,29].

Despite the demonstration of excellent agreement between theory and the new simulation results, substantive disparity would still appear to remain between the two aforementioned approaches

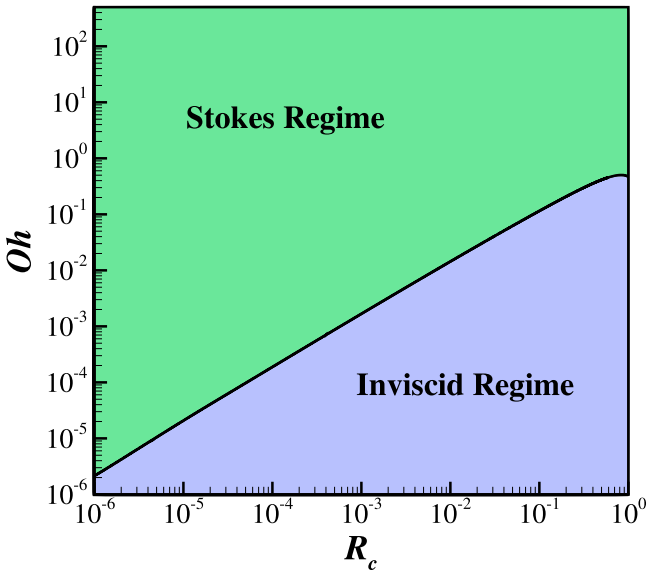


FIG. 11. Phase diagram in the space of Ohnesorge number and crossover radius, $(\mathrm{Oh}, R_c)$, of drop coalescence in a dynamically passive fluid, e.g., a gas such as air, showing the regimes of coalescence and the conditions for transitions between them. Following the occurrence of the space-time singularity when two drops have just touched at a point, coalescence will always begin in the Stokes regime and the dynamics will either transition to the inviscid regime when the minimum radius of the neck connecting the drops exceeds the crossover radius or terminate with the two drops having fully coalesced.

and experiments. However, by varying the initial separation between, or the height of the bridge connecting, the two drops in the simulations, a linear scaling regime that had heretofore been referred to as the ILV regime [29] has been reproduced. Furthermore, it has been demonstrated that this linear regime is more akin to a Taylor-Culick-type regime whose existence and duration are purely consequences of the use of an initial bridge of finite size that poorly approximates the point contact condition that is a cardinal feature of the coalescence singularity. Indeed, it has been demonstrated that such a linear regime does in fact arise even in simulations involving Stokes flow where inertia has been removed from the equations or set equal to zero. Despite demonstrating that the ILV regime does not exist as an asymptotic regime of coalescence, if one looks at the dynamics on larger scales of the order of the drop radius $\tilde{R}$, it has been shown that the flow fields within drops at intermediate values of Oh qualitatively differ from those in the inviscid or the Stokes regimes even though the growth of the neck—the bridge connecting the drops—reliably follows the Stokes theory after two drops have touched and begun to merge into one. This point has then been further investigated by quantitatively measuring and/or characterizing the global or macroscopic motion of the drops. That analysis has shown that although for values of $\mathrm{Oh} < 1$ the global dynamics does not match what would be expected from Stokes flow theory and, furthermore, even after the movement of the drops when viewed from a global perspective transitions from this intermediate regime to the Stokes regime, the local dynamics or the scaling behavior exhibited by the growing bridge remains unaffected and follows Stokes theory.

A number of complicating factors may arise during the coalescence of two drops even in a gas, e.g., air, in real life situations that may limit the applicability of the phase diagram shown in Fig. 11. First, many of the applications used in Sec. I for motivating the computational study carried out in this paper involve drops of radii of 1 mm or smaller. Therefore, for two spherical drops of radius of 1 mm that are initially joined by a bridge of dimensionless radius of $10^{-6}$, the dimensional value of the bridge radius would equal 1 nm. Hence, the bridge height and radius of curvature at

that instant would be orders of magnitude smaller than molecular/atomic length scales. Therefore, the continuum mechanical description used in this paper would be inapplicable at such small length scales. Even for length scales above molecular/atomic ones but ones that are of the order of hundreds of nanometers or less, it has been suggested that van der Waals forces can become important and alter the scaling behavior that is reported in this paper [31]. Furthermore, given the large number of experimental studies in which an initial linear regime has been observed, it is possible that the singular initial conditions of two spheres just touching at a point may not be readily realizable in real life situations. This linear regime seen in experiments has been attributed in Sec. III to the unknown or unknowable consequence of having an initial connecting bridge of finite size whose dimensions may be difficult or even impossible to measure in practice due to the smallness of the length scales involved in the problem. However, knowing the true origin of this linear regime has led to a more complete understanding of transitions that can take place from this linear regime to either an inertial or a viscous regime, and that the nature of these transitions depends solely on the geometry of the initial conditions and not on any intrinsic properties of the fluids. In addition to a finite-size bridge, the speed at which the drops are brought together can also affect the coalescence dynamics due to the deformation of the interface caused by the initial motion of the drops.

The dynamics of coalescence has been analyzed in this paper assuming that the region exterior to the two drops is vacuum (void) or a dynamically passive gas that exerts a constant pressure on the drops. However, the dynamics of the outer fluid may also become significant depending on the values of both the ratio of the viscosities of the two fluids and the ratio of their densities. Eggers *et al.* [23] have concluded that even when the ratio of the viscosity of the inner fluid to that of the outer fluid is large, as when two drops coalesce in air, the existence of the outer fluid must become important as $R_{\min} \to 0$. In their study, an estimate is provided that the dynamics of the outer fluid can be significant when $R_{\min} \leqslant M^{2/3}$ where $M \equiv \mu_{\text{outer}}/\mu_{\text{inner}}$ ($\mu_{\text{outer}}$ and $\mu_{\text{inner}}$ stand for the viscosity of the outer and the inner fluids). Therefore, for two water drops coalescing in air at room temperature and pressure, $R_{\min} = 4.6 \times 10^{-2}$, whereas for two pure glycerol drops, $R_{\min} = 4.6 \times 10^{-4}$. Thus, for two drops of 1 mm radius, the dynamics of the outer fluid cannot be neglected when the minimum neck radius is below 46 $\mu$m when the drop liquid is water but the outer fluid's dynamics can be neglected as long as the neck radius is larger than about 460 nm when the drop liquid is pure glycerol. Similarly, one would also expect the density ratio to play a role in the coalescence dynamics under certain conditions. In situations in which the outer fluid is denser than the inner fluid, it is likely that any coalescence event that begins in a Stokes regime set by the inner fluid would then transition to an inertial regime determined by the outer rather than the inner fluid. This expectation is based on the fact that since the characteristic length scale of the inertial regime in bubble coalescence is the same as the characteristic length scale in the inertial regime in drop coalescence [42,51], the value of the density ratio would then determine which of the phases would be the dominant one as the drops coalesce. However, both of the aforementioned expectations have yet to be confirmed through simulation, and hence efforts directed at verifying them constitute logical and worthy extensions of this work.

In this paper, a new meshing technique has been used such that the domain is divided by a dynamic algebraic surface into two separate regions where the locations of the mesh or grid points in each region can be determined by solving the elliptic mesh generation equations. This algebraic division of the domain or the mesh allows greater control of the density of the mesh in either region. Indeed, this approach makes it possible for the region near the singularity to be highly densified while the body of the drop can remain relatively sparsely discretized, thereby both lowering the computation time and allowing for investigation of smaller values of the initial bridge radius $R_0$. Furthermore, the dividing surface or line is allowed to move in time in accordance with the dynamics of the problem, e.g., as a function of $R_{\min}$ in the present case, and the concept is thus suitable for use in any physical situation in which largely disparate length scales can occur [42,59,60].

**ACKNOWLEDGMENT**

The authors thank the Purdue Process Safety and Assurance Center (P2SAC) for financial support.

[1] D. F. Evans and H. Wennerström, *Colloidal Domain* (VCH Publishers, New York, 1994).
[2] A. Saboni, C. Gourdon, and A. K. Chesters, Drainage and rupture of partially mobile films during coalescence in liquid-liquid systems under a constant interaction force, J. Colloid Interface Sci. **175**, 27 (1995).
[3] J. S. Eow and M. Ghadiri, Electrostatic enhancement of coalescence of water droplets in oil: A review of the technology, Chem. Eng. J. **85**, 357 (2002).
[4] J. S. Eow, M. Ghadiri, A. O. Sharif, and T. J. Williams, Electrostatic enhancement of coalescence of water droplets in oil: A review of the current understanding, Chem. Eng. J. **84**, 173 (2001).
[5] X. Zhang, O. A. Basaran, and R. M. Wham, Theoretical prediction of electric-field enhanced coalescence of spherical drops, AIChE J. **41**, 1629 (1995).
[6] K. J. Ptasinski and P. J. A. M Kerkhof, Electric field driven separations: Phenomena and applications, Separation Sci. Technol. **27**, 995 (1992).
[7] C. H. Byers and A. Amarnath, Understand the potential of electro-separations, Chem. Eng. Prog. **91**, 63 (1995).
[8] M. Harris, W. Sisson, and O. A. Basaran, Computation, visualization, and chemistry of electric field-enhanced production of ceramic precursor powders, MRS Proc. **271**, 945 (1992).
[9] S. Kumar, G. Narsimhan, and D. Ramkrishna, Coalescence in creaming emulsions. existence of a pure coalescence zone, Ind. Eng. Chem. Res. **35**, 3155 (1996).
[10] N. Ashgriz and J. Y. Poo, Coalescence and separation in binary collisions of liquid drops, J. Fluid Mech. **221**, 183 (1990).
[11] R. D. Reitz and R. Diwakar, Effect of drop breakup on fuel sprays, SAE Technical Paper (1986).
[12] D. Segal, *Chemical Synthesis of Advanced Ceramic Materials* (Cambridge University Press, New York, 1989).
[13] H. Djohari, J. I. Martínez-Herrera, and J. J. Derby, Transport mechanisms and densification during sintering: I. Viscous flow versus vacancy diffusion, Chem. Eng. Sci. **64**, 3799 (2009).
[14] M. Konno, K. Arai, and S. Saito, The effect of stabilizer on coalescence of dispersed drops in suspension polymerization of styrene, J. Chem. Eng. Jpn. **15**, 131 (1982).
[15] T. M. Tran, F. Lan, C. S. Thompson, and A. R. Abate, From tubes to drops: Droplet-based microfluidics for ultrahigh-throughput biology, J. Phys. D **46**, 114004 (2013).
[16] F. H. Ludlam, The production of showers by the coalescence of cloud droplets, Q. J. R. Meteorol. Soc. **77**, 402 (1951).
[17] J. D. Sartor, Electricity and rain, Phys. Today **22**(8), 45 (1969).
[18] W. D. Ristenpart, J. C. Bird, A. Belmonte, F. Dollar, and H. A. Stone, Non-coalescence of oppositely charged drops, Nature (London) **461**, 377 (2009).
[19] C. K. Haluska, K. A. Riske, V. Marchi-Artzner, J.-M. Lehn, R. Lipowsky, and R. Dimova, Time scales of membrane fusion revealed by direct imaging of vesicle fusion with high temporal resolution, Proc. Natl. Acad. Sci. USA **103**, 15841 (2006).
[20] C. P. Brangwynne, T. J. Mitchison, and A. A. Hyman, Active liquid-like behavior of nucleoli determines their size and shape in *Xenopus laevis* oocytes, Proc. Natl. Acad. Sci. USA **108**, 4334 (2011).
[21] R. W. Hopper, Coalescence of two equal cylinders: Exact results for creeping viscous plane flow driven by capillarity, J. Am. Ceram. Soc. **67**, C-262 (1984).
[22] R. W. Hopper, Plane stokes flow driven by capillarity on a free surface, J. Fluid Mech. **213**, 349 (1990).
[23] J. Eggers, J. R. Lister, and H. A. Stone, Coalescence of liquid drops, J. Fluid Mech. **401**, 293 (1999).
[24] S. T. Thoroddsen, T. G. Etoh, and K. Takehara, The coalescence speed of a pendent and a sessile drop, J. Fluid Mech. **527**, 85 (2005).

[25] D. G. A. L. Aarts and H. N. W. Lekkerkerker, Droplet coalescence: Drainage, film rupture and neck growth in ultralow interfacial tension systems, J. Fluid Mech. **606**, 275 (2008).
[26] W. Yao, H. J. Maris, P. Pennington, and G. M. Seidel, Coalescence of viscous liquid drops, Phys. Rev. E **71**, 016309 (2005).
[27] J. C. Burton and P. Taborek, Role of Dimensionality and Axisymmetry in Fluid Pinch-Off and Coalescence, Phys. Rev. Lett. **98**, 224502 (2007).
[28] J. D. Paulsen, J. C. Burton, and S. R. Nagel, Viscous to Inertial Crossover in Liquid Drop Coalescence, Phys. Rev. Lett. **106**, 114501 (2011).
[29] J. D. Paulsen, J. C. Burton, S. R. Nagel, S. Appathuri, M. T. Harris, and O. A. Basaran, The inexorable resistance of inertia determines the initial regime of drop coalescence, Proc. Natl. Acad. Sci. USA **109**, 6857 (2012).
[30] J. E. Sprittles and Y. D. Shikhmurzaev, Coalescence of liquid drops: Different models versus experiment, Phys. Fluids **24**, 122105 (2012).
[31] J. D. Paulsen, Approach and coalescence of liquid drops in air, Phys. Rev. E **88**, 063010 (2013).
[32] J. E. Sprittles and Y. D. Shikhmurzaev, A parametric study of the coalescence of liquid drops in a viscous gas, J. Fluid Mech. **753**, 279 (2014).
[33] J. E. Sprittles and Y. D. Shikhmurzaev, Dynamics of liquid drops coalescing in the inertial regime, Phys. Rev. E **89**, 063008 (2014).
[34] L. Baroudi, M. Kawaji, and T. Lee, Effects of initial conditions on the simulation of inertial coalescence of two drops, Comput. Math. Appl. **67**, 282 (2014).
[35] J. D. Paulsen, R. Carmigniani, A. Kannan, J. C. Burton, and S. R. Nagel, Coalescence of bubbles and drops in an outer fluid, Nat. Commun. **5**, 3182 (2014).
[36] X. Xia, C. He, and P. Zhang, Universality in the viscous-to-inertial coalescence of liquid droplets, Proc. Natl. Acad. Sci. USA **116**, 23467 (2019).
[37] L. Duchemin, J. Eggers, and C. Josserand, Inviscid coalescence of drops, J. Fluid Mech. **487**, 167 (2003).
[38] H. N. Oguz and A. Prosperetti, Surface-tension effects in the contact of liquid surfaces, J. Fluid Mech. **203**, 149 (1989).
[39] A. Menchaca-Rocha, A. Martínez-Dávalos, R. Núñez, S. Popinet, and S. Zaleski, Coalescence of liquid drops by surface tension, Phys. Rev. E **63**, 046309 (2001).
[40] K. Fezzaa and Y. Wang, Ultrafast X-Ray Phase-Contrast Imaging of the Initial Coalescence Phase of Two Water Droplets, Phys. Rev. Lett. **100**, 104501 (2008).
[41] S. C. Case and S. R. Nagel, Coalescence in Low-Viscosity Liquids, Phys. Rev. Lett. **100**, 084503 (2008).
[42] C. R. Anthony, P. M. Kamat, S. S. Thete, J. P. Munro, J. R. Lister, M. T. Harris, and O. A. Basaran, Scaling laws and dynamics of bubble coalescence, Phys. Rev. Fluids **2**, 083601 (2017).
[43] M. S. Gockenbach, *Understanding and Implementing the Finite Element Method* (Society for Industrial and Applied Mathematics, Philadelphia, 2006).
[44] J. Q. Feng and O. A. Basaran, Shear flow over a translationally symmetric cylindrical bubble pinned on a slot in a plane wall, J. Fluid Mech. **275**, 351 (1994).
[45] P. K. Notz and O. A. Basaran, Dynamics and breakup of a contracting liquid filament, J. Fluid Mech. **512**, 223 (2004).
[46] K. N. Christodoulou and L. E. Scriven, Discretization of free surface flows and other moving boundary problems, J. Comput. Phys. **99**, 39 (1992).
[47] P. P Bhat, O. A. Basaran, and M. Pasquali, Dynamics of viscoelastic liquid filaments: Low capillary number flows, J. Non-Newtonian Fluid Mech. **150**, 211 (2008).
[48] P. M. Gresho and R. L. Sani, *Incompressible Flow and the Finite Element Method* (John Wiley & Sons, New York, 2000).
[49] P. Hood, Frontal solution program for unsymmetric matrices, Intl. J. Numer. Methods Eng. **10**, 379 (1976).
[50] C. R. Anthony, P. M. Kamat, M. T. Harris, and O. A. Basaran, Dynamics of contracting filaments, Phys. Rev. Fluids **4**, 093601 (2019).
[51] J. P. Munro, C. R. Anthony, O. A. Basaran, and J. R. Lister, Thin-sheet flow between coalescing bubbles, J. Fluid Mech. **773**, R3 (2015).

[52] C. R. Anthony, Dynamics of retracting films and filaments near singularities, Ph.D. thesis, Purdue University, 2017.
[53] J. R. Castrejón-Pita, A. A. Castrejón-Pita, S. S. Thete, K. Sambath, I. M. Hutchings, J. Hinch, J. R. Lister, and O. A. Basaran, Plethora of transitions during breakup of liquid filaments, Proc. Natl. Acad. Sci. USA **112**, 4582 (2015).
[54] F. E. C. Culick, Comments on a ruptured soap film, J. Appl. Phys. **31**, 1128 (1960).
[55] G. I. Taylor, The dynamics of thin sheets of fluid. III. Disintegration of fluid sheets, Proc. R. Soc. London A **253**, 313 (1959).
[56] É. Reyssat and D. Quéré, Bursting of a fluid film in a viscous environment, Europhys. Lett. **76**, 236 (2006).
[57] S. T. Thoroddsen, M. J. Thoraval, K. Takehara, and T. G. Etoh, Micro-bubble morphologies following drop impacts onto a pool surface, J. Fluid Mech. **708**, 469 (2012).
[58] S. C. Case, Coalescence of low-viscosity fluids in air, Phys. Rev. E **79**, 026307 (2009).
[59] K. Sambath, V. Garg, S. S. Thete, H. J. Subramani, and O. A. Basaran, Inertial impedance of coalescence during collision of liquid drops, J. Fluid Mech. **876**, 449 (2019).
[60] R. T. Collins, K. Sambath, M. T. Harris, and O. A. Basaran, Universal scaling laws for the disintegration of electrified drops, Proc. Natl. Acad. Sci. USA **110**, 4905 (2013).